

The Supernova Remnants IC 443 and VRO 42.05.01: Fast Filaments and High-velocity Gas

T. A. Lozinskaya

Sternberg Astronomical Institute, Moscow, U.S.S.R.

Abstract

Interferometric H α observations have been made of faint filaments and high-velocity diffuse gas in the supernova remnants IC 443 and VRO 42.05.01. In both cases the implied expansion velocities are substantially higher than those obtained from the velocities of the bright filaments.

1. Introduction

It is well known that there is in general a wide divergence between the radial velocities of the filaments in a supernova remnant and the blast-wave velocity necessary to produce the temperature inferred from X-ray observations. This is attributed to irregularities in the distribution of the interstellar medium. In the present paper the velocity structures of two remnants, IC 443 and VRO 42.05.01 are examined, with particular attention being given to the faint filaments of highest velocity and the faint emission from diffuse high-velocity gas.

2. IC 443

The mean expansion velocity of the bright NE. part of the filamentary shell of IC 443 has been found to be about 65 km s^{-1} , but some faint filaments have been shown to possess radial velocities as high as 150 km s^{-1} (Lozinskaya 1969, 1975*a*, 1975*b*). On the other hand, soft X-ray observations of the nebula are well fitted by a thermal spectrum with temperature $T_x = 10^7 \text{ K}$ (Malina *et al.* 1976; Parker *et al.* 1977) which corresponds to a shock velocity of about 800 km s^{-1} for an adiabatic blast wave in a uniform medium. McKee and Cowie (1975) and Bychkov and Pikel'ner (1975) have shown that such a large discrepancy in velocities can be understood if the blast wave is propagating through a cloudy interstellar medium; the blast wave then accelerates the interstellar clouds to a fraction of its velocity. Since the velocity of the clouds is determined by their density, the velocity of the faint filaments must be almost as high as the gas velocity behind the blast wave.

Taking into account the above explanation, I have continued a program of interferometric H α observations of IC 443 in order to evaluate the velocities of the fastest filaments in the bright NE. and faint SW. parts of the nebula and to search for high-velocity gas. (Kirshner and Taylor (1976) found faint H α emission in the Cygnus Loop at velocities of about 300 km s^{-1} inferred from X-ray spectra; these results have been confirmed by Doroshenko and Lozinskaya (1977).) A Palomar sky survey red print of IC 443 is shown in Fig. 1.

Observations

Interferometric $H\alpha$ observations were carried out with a high-contrast Fabry-Perot etalon and a contact image converter attached to the Cassegrain focuses of a 0.50, a 1.25 and a 2.60 m reflector. The 50 mm diameter etalon plates had a reflection coefficient of 95% and a separation of 0.149 mm, which provided a free spectral range of about 660 km s^{-1} in velocity scale. The linear dispersion was $5\text{--}7 \text{ \AA mm}^{-1}$, the actual spectral resolution corresponding to $15\text{--}20 \text{ km s}^{-1}$. An $H\alpha$ interference filter with a FWHM of 18 \AA was used to isolate the $H\alpha$ from the [NII] lines, the interference ring of the 6584 \AA [NII] line being situated at about -390 and $+270 \text{ km s}^{-1}$ relative to the $H\alpha$ rings. Angular resolution for the 0.50, 1.25 and 2.60 m reflectors corresponded to $20\text{--}25''$, $10\text{--}15''$ and $4\text{--}8''$ respectively. The exposure times ranged from 1^{h} to $1^{\text{h}} 30^{\text{m}}$.

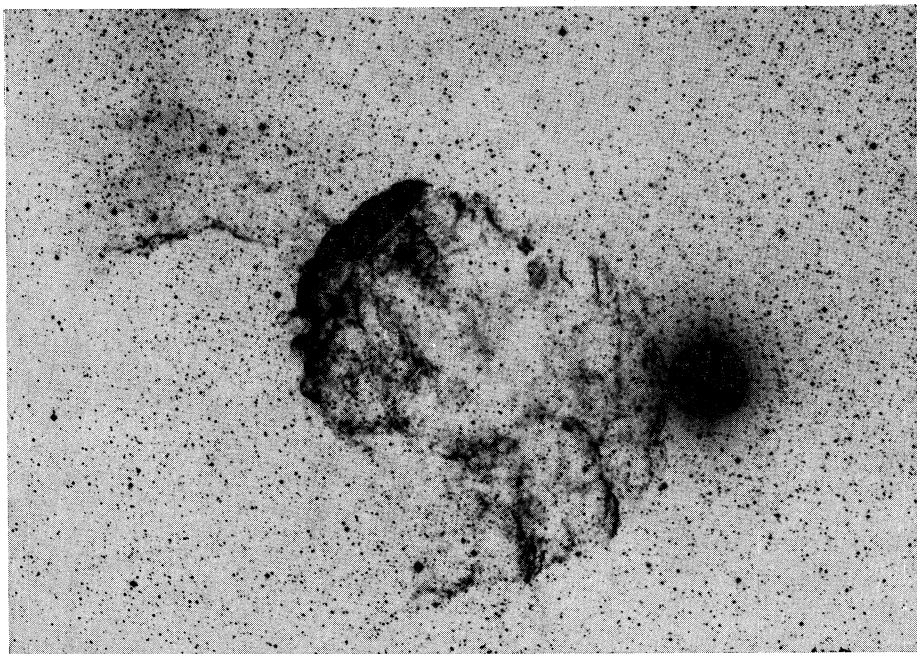


Fig. 1. Palomar sky survey red print of IC 443.

Fast Filaments in IC 443 Shell

Typical $H\alpha$ profiles obtained for IC 443 (illustrated by photometric scans in Fig. 2) show a rather complicated structure. It was not possible to fit accurately a small number of gaussian components to these profiles. The one feature which is evident over the entire nebula is the brightest 'zero' component ($|V_r| \leq 30 \text{ km s}^{-1}$), which is produced partly by dense slowly accelerated filaments and partly by the galactic $H\alpha$ background. In addition to the zero component, there are 'shifted' components in complicated $H\alpha$ profiles at some locations within the nebula; these are emitted by fast-moving filaments, their intensity being about 30%–80% of the maximum intensity of the zero component.

In order to estimate the highest velocities of the fast filaments, I evaluated the radial velocity of the most shifted (positive or negative) distinct component in every complicated $H\alpha$ profile. The data obtained are shown in Fig. 3a, in which the radial velocities of the most shifted components are plotted against distance from the SNR's centre. Since the spatial shape of the IC 443 filamentary system cannot be represented by a spherical shell, the distance is plotted in dimensionless form relative to the remnant's maximum radius R_{\max} at the same position angle. The left- and right-hand

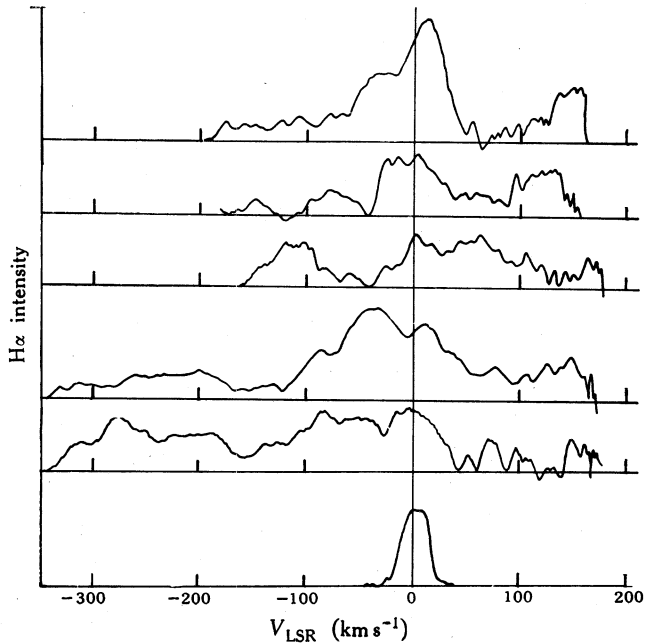


Fig. 2. Examples of typical $H\alpha$ line profiles for IC 443. The intensities are in relative units.

parts of Fig. 3a illustrate the observational data for the bright NE. and faint SW. sectors of IC 443 respectively. The radial velocities of separate filaments of the SNR are found to vary in the range of $-220 \leq V_{\text{LSR}} \leq 220 \text{ km s}^{-1}$. (The accuracy of the determination corresponds to $\pm 10 \text{ km s}^{-1}$.) To take into account the geometrical projection of the velocity, I have used the Kompaneets (1960) solution for a point explosion in a medium with an exponential density distribution. The optical, radio and X-ray shapes of IC 443 and the HI cloud adjacent to the NE. part of the shell are evidence for a strong density gradient, and in this case the standard self-similar solution does not fit the blast-wave propagation. Gulliford (1974) has proven that the visual remnant's shape is best fitted to a shock-wave radius given by

$$R_s(\theta) = R_0 \{1 + CR_0 H^{-1} \cos \theta\} \quad (1)$$

in a medium characterized by a density variation of the form

$$\rho(Z) = \rho_0 \exp(-Z/H). \quad (2)$$

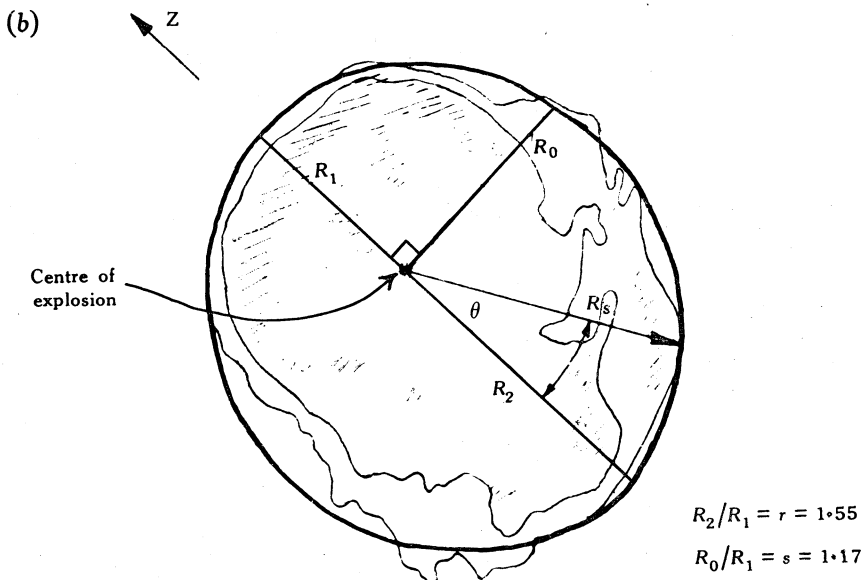
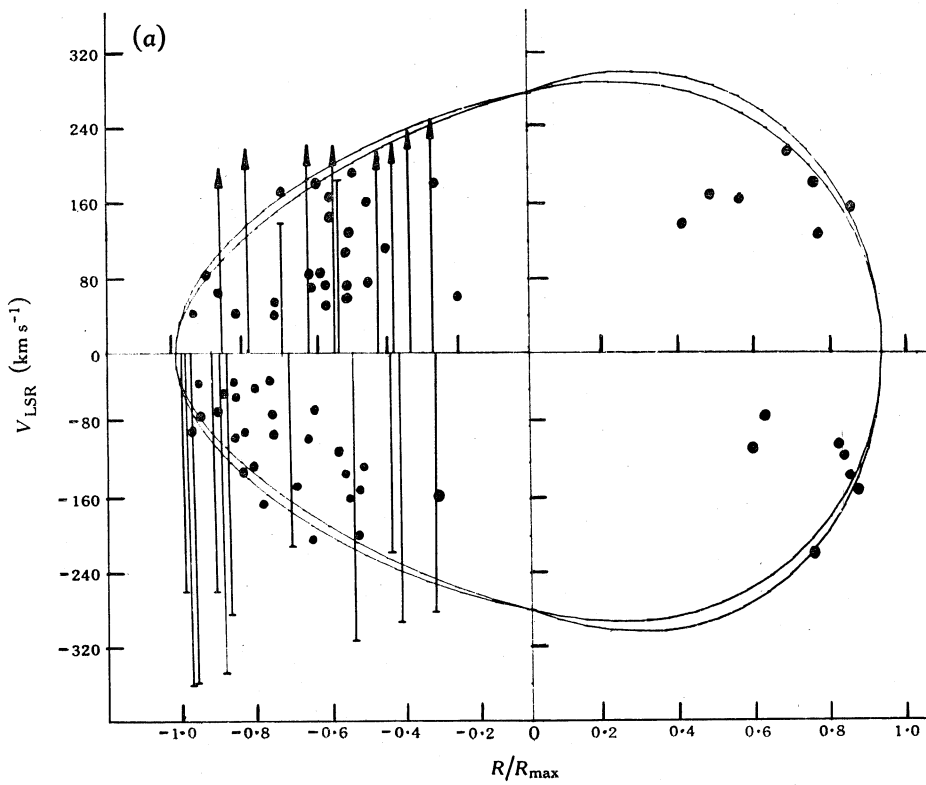


Fig. 3. Kompaneets curves fitted to experimental data:

(a) A plot of the present measurements for the radial velocities (points) of the most shifted components in $H\alpha$ line profiles for IC 443 versus distance from the SNR's centre relative to the remnant's maximum radius. Vertical bars denote velocity ranges for the high-velocity gas; those terminated by arrows are truncated due to instrumental limitation. NE. is to the left and SW. to the right.

(b) Gulliford's (1974) best-fitted solution (bold curve) superimposed on a representation of IC 443 showing the prominent optical and radio features.

The corresponding shock-wave velocity is given by

$$V_s(\theta) = V_0 \{1 + 2CR_0 H^{-1} \cos \theta\}. \quad (3)$$

Here θ is the polar angle measured from the centre of the explosion (as shown in Fig. 3*b*); $Z = R_s(\theta) \cos \theta$; the constant $C = 0.186$; R_0 and V_0 are the standard shock-wave radius and velocity for a uniform medium and are given by

$$R_0 = (2.2 E_0 / \rho_0)^{1/5} t^{2/5} \quad \text{and} \quad V_0 = \frac{2}{5} R_0 / t,$$

with E_0 the initial blast energy and t the time since the blast; while the scale height $H = 0.85 R_0$, as determined by the visual remnant's shape only. However, the actual shell may be more asymmetrical than is suggested by these equations if there is an inclination effect. The only possibility for evaluating such an effect is to search the radial velocity diagram for a typical asymmetry of positive and negative velocities along the major axis of the nebula.

Using equations (2) and (3) I have computed predicted radial velocity variations with distance from the SNR's centre for a set of different 'inclined' egg-shape shells having the same visual asymmetry in projection on the sky. An egg-shape shell with its major axis normal to the line of sight has proven to be the best fit to the velocity data. Statistical reduction of the radial velocity data gives $V_0 = 280 \pm 30 \text{ km s}^{-1}$, determined by the fastest filaments of the SNR. The computed radial velocity variation over the egg-shape surface (Kompaneets solution) with the major axis normal to the line of sight and with $H = 0.85 R_0$, $R_0 = 9 \text{ pc}$ and $V_0 = 280 \text{ km s}^{-1}$ is shown in Fig. 3*a* by the two curves, which correspond to extreme cases of radial velocity variation for different cross sections of the surface.

Substituting $V_0 = 280 \text{ km s}^{-1}$ into equation (3) gives a post-shock gas velocity V_{gas} that ranges from $V_{\text{min}} = 150 \text{ km s}^{-1}$ to V_0 for the NE. part and from V_0 to $V_{\text{max}} = 400 \text{ km s}^{-1}$ for the SW. part of the nebula. The corresponding shock-wave velocity $V_s = \frac{4}{3} V_{\text{gas}}$ reaches $200\text{--}370 \text{ km s}^{-1}$ in the NE. sector and $370\text{--}530 \text{ km s}^{-1}$ in the SW. sector. This gives a post-shock temperature T_s in the range $(0.5\text{--}1.5) \times 10^6 \text{ K}$ for the NE. sector and $(1.5\text{--}3.0) \times 10^6 \text{ K}$ for the SW. sector. The previously quoted 'X-ray' temperature $T_x = 10^7 \text{ K}$ may be somewhat overestimated because of plasma reheating and an internal density increase due to a reflected shock wave in the strong density gradient.

High Velocity Gas

I have detected low surface-brightness $\text{H}\alpha$ emission from high-velocity gas in the bright NE. sector of the nebula. The positive velocities reach $V_{\text{LSR}} = 240 \text{ km s}^{-1}$, which is a lower limit because of instrumental limitations. The high-velocity gas was found to be distinguishable in $\text{H}\alpha$ for the range of negative velocities: $V_{\text{LSR}} \geq -350$ to -400 km s^{-1} . Taking into account the geometrical projection, one can then conclude that the high-velocity gas moves outward from the SNR's centre with a velocity of about $400\text{--}500 \text{ km s}^{-1}$. Fig. 4 indicates the location of the high-velocity gas on a schematic diagram of the nebula. The high-velocity gas was not visible on every interference photograph, its intensity being about 3%–5% of the intensity of the zero component. The shape of the high-velocity $\text{H}\alpha$ profile is flat; it seems to be an

amorphous background under the zero and shifted components (see Fig. 2). Although the high-velocity H α emission is visible in the region of the bright filaments of the nebula, it does not show a fine filamentary structure as do the shifted components. This leads us to the assumption that high-velocity H α emission originates in a diffuse medium near the filaments. The same conclusion was reached by Doroshenko and Lozinskaya (1977) for the Cygnus Loop. McKee *et al.* (1978) have explained the diffuse gas in terms of a second-stage acceleration of early-shocked small-massive interstellar clouds by the flow of shocked interstellar material past the cloud.



Fig. 4. Schematic representation of IC 443 showing the localization of the high-velocity gas. Positive and negative velocities are shown by vertical and horizontal lines respectively.

To show that the above interpretation of the high-velocity gas is applicable to IC 443, let us set the shock-wave radius to $R_s = 9$ pc, the mean dimension of the clouds to 0.2–0.3 pc, and the ambient cloud density to $\rho_c \approx 100\text{--}200\text{ cm}^{-3}$ as measured by optical observations. The evaluation of the shocked intercloud density ρ_{si} is rather uncertain. We have $\rho_{si} = 4\rho_0 \approx 1\text{ cm}^{-3}$ in accordance with the X-ray luminosity, or $\rho_{si} \approx 40\text{ cm}^{-3}$ in agreement with the 21 cm data. Using numerical solutions of cloud-dynamics equations obtained by McKee *et al.* (1978) for two cases (evaporative and non-evaporative) we can conclude the following: given a present velocity for the intercloud material immediately behind the blast wave of about 700 km s^{-1} (as measured by X-ray spectra), the clouds would have reached the observed velocity of about $400\text{--}500\text{ km s}^{-1}$ if they were overtaken by the shock when its radius was about 40%–80% of the present size.

Conclusions

The H α observations of the internal motions in IC 443 are in good agreement with the model of blast-wave propagation in the interstellar medium for both the strong large-scale gradient and the small-scale fluctuations of density. The radial velocity diagram for the bright filaments gives an egg-shaped shell with its major axis normal to the line of sight, a scale height of density gradient $H \approx 7$ pc and a standard gas velocity $V_0 = 280\text{ km s}^{-1}$. The corresponding shock velocity $V_s = 370\text{ km s}^{-1}$

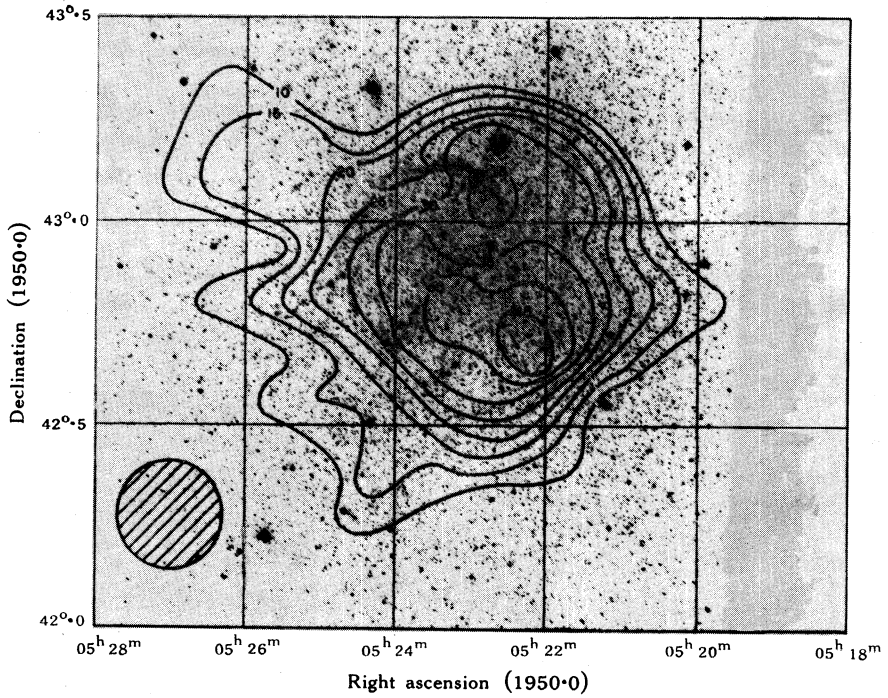


Fig. 5. Palomar sky survey print of VRO42.05.01, with the 610.5 MHz radio contours of Dickel *et al.* (1965) superimposed.

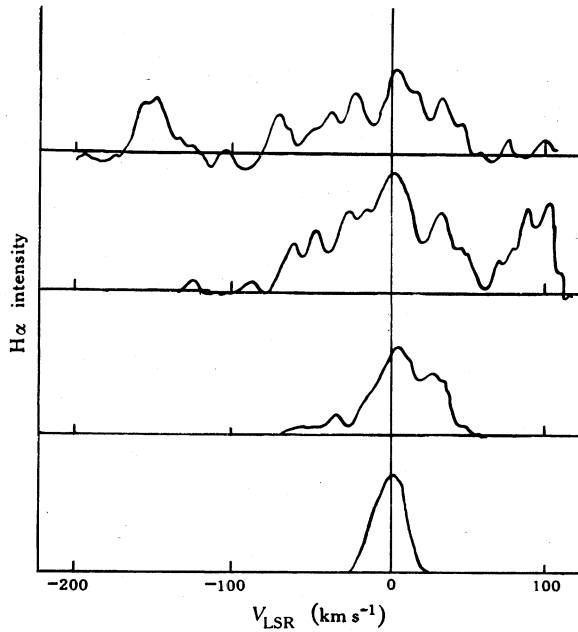


Fig. 6. Examples of typical H α line profiles for VRO42.05.01. The intensities are in relative units.

reduces the SNR's age as determined by the velocities of the fastest optical filaments to $t_{\text{opt}} = 2R_s/5V_s = 9 \times 10^3$ years instead of 6×10^4 years, as previously estimated by the author from the mean expansion velocity of the bright NE. part of the optical shell. The 'X-ray' age of the SNR, $t_x = 3 \times 10^3$ years, may be somewhat underestimated because of plasma reheating by a reflected shock wave in the strong density gradient.

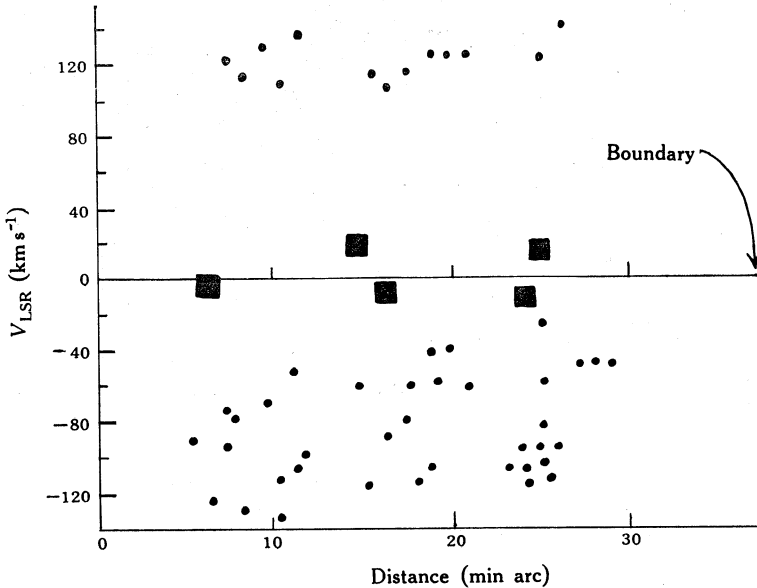


Fig. 7. Plot of the present measurements for the radial velocities of the most shifted components in $H\alpha$ line profiles for VRO 42.05.01 versus angular distance from the SNR's centre. Data for the five brightest filaments are denoted by squares.

3. VRO 42.05.01

The old supernova remnant VRO 42.05.01 is identified with the faint nebula Sh 224 (Sharpless 1959) and is shown in Fig. 5. Its five brightest optical filaments have been demonstrated to move from the SNR's centre with a velocity of less than $35\text{--}40 \text{ km s}^{-1}$, while evaluation of the $H\alpha$ -line half-widths from filaments and diffuse regions in the nebula yields a cloud shock velocity as high as $50\text{--}100 \text{ km s}^{-1}$ (Lozinskaya 1971, 1978). The blast-wave velocity is therefore in excess of 100 km s^{-1} . I present below new direct evidence for a high expansion velocity for the SNR. This has been obtained from interferometric observations with a high-contrast Fabry-Perot etalon and a contact image converter that were carried out in the $H\alpha$ and [NII] (6584 \AA) lines. The interferometer's parameters and the reduction method are described in Section 2.

Typical $H\alpha$ profiles of the nebula (illustrated in Fig. 6) exhibit a rather complicated multicomponent shape. The brightest zero component ($|V_{\text{LSR}}| \leq 30 \text{ km s}^{-1}$) is visible all over the nebula, while shifted positive and negative components are emitted at some locations within the SNR. Radial velocities for the most shifted distinct components in every complicated $H\alpha$ profile were estimated as in Section 2. The data obtained are plotted in Fig. 7 against distance from the SNR's centre ($\alpha_{1950} = 5^{\text{h}} 23^{\text{m}}$,

$\delta_{1950} = 42^\circ \cdot 8$). The mean radial velocities of the five brightest filaments of the nebula are denoted by full squares. The geometrical projection effect is not important since the optical nebula is concentrated in the central part of the nonthermal radio source. The data illustrated by Fig. 7 show that the radial velocities of separate faint filaments and diffuse gaseous clouds lie in the range $140 \geq V_{\text{LSR}} \geq -130 \text{ km s}^{-1}$. The present [NII]-line observations are in accordance with the H α -line data; the reduction method does not allow one to obtain the absolute radial velocities, but I have made relative estimates of velocity range. The radial velocity as determined by [NII]-line observation is found to vary in a range of about $\Delta V_2 = 250 \text{ km s}^{-1}$. The internal motions are distributed in VRO 42.05.01 in a manner similar to the situation in other old SNRs such as IC 443 and the Cygnus Loop: a system of slow-moving bright filaments with faint high-velocity filamentary and amorphous condensations. The gas velocity of about 140 km s^{-1} corresponds to a shock-wave velocity of 200 km s^{-1} . So, in spite of the slow filaments, the shock-wave velocity is high enough for us to assume that the SNR is still in the adiabatic phase of its expansion. This implies an age for $V_s = 200 \text{ km s}^{-1}$ and $R = 28 \text{ pc}$ (Ilovaisky and Lequeux 1972) of about 60 000 years, and a value for E_0/ρ_0 of $6 \times 10^{50} \text{ erg cm}^{-3}$.

References

- Bychkov, K. V., and Pikel'ner, S. B. (1975). *Pis'ma Astron. Zh.* **1**, 29.
 Dickel, J. R., McGuire, J. P., and Yang, K. S. (1965). *Astrophys. J.* **142**, 798.
 Doroshenko, V. T., and Lozinskaya, T. A. (1977). *Pis'ma Astron. Zh.* **3**, 112.
 Gulliford, P. (1974). *Astrophys. Space Sci.* **31**, 241.
 Ilovaisky, S. A., and Lequeux, J. (1972). *Astron. Astrophys.* **18**, 169.
 Kirshner, R. P., and Taylor, R. (1976). *Astrophys. J.* **208**, 183.
 Kompaneets, A. S. (1960). *Sov. Phys. Dokl.* **5**, 46.
 Lozinskaya, T. A. (1969). *Astron. Zh.* **46**, 245.
 Lozinskaya, T. A. (1971). *Astron. Zh.* **48**, 1145.
 Lozinskaya, T. A. (1975a). *Astron. Zh.* **52**, 39.
 Lozinskaya, T. A. (1975b). *Pis'ma Astron. Zh.* **1**, 25.
 Lozinskaya, T. A. (1978). *Astron Astrophys.* **64**, 123.
 McKee, C. F., and Cowie, L. L. (1975). *Astrophys. J.* **195**, 715.
 McKee, C. F., Cowie, L. L., and Ostriker, J. P. (1978). *Astrophys. J. Lett.* **219**, L23.
 Malina, R., Lampton, M., and Bowyer, S. (1976). *Astrophys. J.* **201**, 894.
 Parker, G. E., Charles, P. A., Culhane, J. L., and Ives, J. C. (1977). *Mon. Not. R. Astron. Soc.* **179**, 55.
 Sharpless, S. (1959). *Astrophys. J. Suppl.* **4**, 257.

